Int. J. Engng Ed. Vol. 10, No. 5, pp. 434–449, 1994
Printed in Great Britain.

0742-0269/91 $3.00+0.00

Electrostatics and Thermostatics: A Connection Between Electrical and Mechanical Engineering*

CHIN C. LEE
DAVID H. CHIEN
Department of Electrical and Computer Engineering, University of California, Irvine, CA 92717, USA

This paper establishes a basic analogy between electrostatics and thermostatics to improve the communication between electrical and mechanical engineers. The analogy further enhances the learning of electrical engineers in thermal problems as well as the learning of mechanical engineers in electrical problems. The analogy is clearly exhibited using a well-designed table, a figure and an example. To reinforce the concept, analytical solutions are derived for a two-dimensional two-layer structure with a strip source of known flux. The solutions together with a new discretization method are used to solve the similar structure with known voltage on the strip electrode. Two practical examples are presented for further illustration and understanding.

INTRODUCTION

DESPITE the similarity between thermostatics and electrostatics, little effort has been devoted to linking these two subjects together. This paper establishes the basic analogy between these two subjects so that mechanical engineers can apply their knowledge in thermostatics to solve the electrostatic problems and electrical engineers can use their knowledge in electrostatics to study the thermostatic problems. Through this analogy, we hope that electrical engineers will become more able to think in thermal terms and mechanical engineers will become more comfortable with electrical terms.

Electrical engineering students learn electrostatics in electromagnetic theory but seldom have a chance to study thermostatics. On the other hand, mechanical engineering students study thermostatics in heat transfer but do not have an opportunity to learn electrostatics. Thus, few students understand both subjects well. Most of them probably are not taught both subjects in school. The basic analogy between two subjects definitely will improve the communications between the electrical and mechanical engineers.

In industries and in applications, electrical problems are almost certainly coupled with thermal problems. Neither electrical engineers nor mechanical engineers can get by without facing both problems. In view of the trend of a concurrent engineering approach to improve design efficiency and reduce design cycle time, understanding of both subjects is highly encouraged. Furthermore, in present products, more different parts are integrated in more systems. This results in more interaction, more interface and more coupling between electrical and thermal problems. Consequently, knowing both subjects well becomes increasingly important and highly desirable.

Mathematically, electrostatic and thermostatic problems share the same Poisson equation. The major mathematical difference between them lies in the boundary conditions, in particular, the prescribed conditions on the sources. For the thermostatic problem, it is usually the flux on the source that is prescribed for the determination of temperature distribution. For the electrostatic problem, however, it is the voltage (temperature) that is given for determining the charge flux (heat flux). In what follows, we first present the basic analogy between electrostatic parameters and thermostatic parameters. This analogy is clearly displayed using a well-designed table, a figure and an example. A two-layer structure with a strip source of know flux is analysed. Analytical temperature solution is derived using Fourier integral transform. A two-layer structure with a strip source of known potential (temperature) is then studied. Analytical solution for the charge flux (heat flux) of this structure is not available. A discretization method is thus formulated to calculate the charge density distribution on the strip source. An electrostatic example of strip transmission line is analysed for illustration purposes. A thermostatic example on the thermal performance of a field effect transistor is presented and discussed. The paper is concluded with a short summary.

* Paper accepted 5 June 1994.

Table 1. Analogy between thermostatics and electrostatics

Thermostatics	Electrostatics I	Electrostatics II
Temperature, T (°C)	Potential, V (Volt)	Potential, V (Volt)
Temperature gradient ∇T (°C/cm)	Electric field $E = -\nabla V$ (V/cm)	Electric field $E = -\nabla V$ (V/cm)
Thermal conductivity K (Watt/cm °C)	Electrical permitivity ε (Coulomb/cm V) or (Farad/cm)	Electrical conductivity κ (A/(cm V)) or (1/(cmΩ))
Heat rate, Q (Watt)	Charge, Q (Coulomb)	Current, I (amp)
Heat rate density q_{th} (Watt/cm³)	Charge density q_e (Coulomb/cm³)	Current density π_c(A/cm³)
Heat flux F (Watt/cm²)	Electrical displacement D (Coulomb/cm²)	Charge flux J (A/cm²)
$F = -K\nabla T$	$D = -\varepsilon\nabla V$	$J = -\kappa\nabla V$
$\nabla \cdot F = q_{th}$	$\nabla \cdot D = q_e$	$\nabla \cdot J = \pi_c$
Thermal conductance	Electrical capacitance	Electrical conductance
$G_{th} = \frac{Q}{T}$ (Watt/°C)	$C = \frac{Q}{V}$ (Coulomb/V)	$G_e = \frac{I}{V}$ (A/V)
Governing Poisson's equation	Governing Poisson's equation	Governing Poisson's equation
$\nabla^2 T = \frac{1}{K} q_{th}$	$\nabla^2 V = \frac{1}{\varepsilon} q_e$	$\nabla^2 V = \frac{1}{\kappa} \pi_c$
Typical boundary condition of source: F is uniform	Typical boundary condition on source: V is uniform	Typical boundary condition on source: V is uniform

ANALOGY BETWEEN THERMOSTATICS AND ELECTROSTATICS

Table 1 exhibits the analogy between thermostatics and electrostatics. Figure 1 shows the corresponding two-dimensional two-layer configurations. Here, we use the terminology 'thermostatics' to describe the steady-state heat conduction problem. As for electrostatics, it is seen from Table 1 that there are two types of electrostatic problems, i.e. electrostatics I and II. Electrostatics I is concerned with the structure which has an electrode between two dielectric media of very low electrical conductivity. One of its major applications is the analysis of strip transmission lines under quasi-TEM approximation [1, 2]. Electrostatics II deals with the structure composed of media having high electrical conductivity. One application is the analysis of electrical resistance of laser diodes [3].

Mathematically, thermostatic and electrostatic problems share the same Poisson equation. The major difference between them lies in the boundary conditions, in particular, the prescribed conditions on the source, as indicated in Table 1 and Fig. 1. For the thermostatic problem as in Fig. 1(a), usually the flux on the heat source is prescribed for determining the temperature distribution. If the flux on the source is uniform, the temperature solution is derivable. For the electrostatic I problems shown in Fig. 1(b), the potential on the source (electrode) is given for calculating the charge density distribution on the electrode and the potential distribution inside the media. With prescribed potential on the

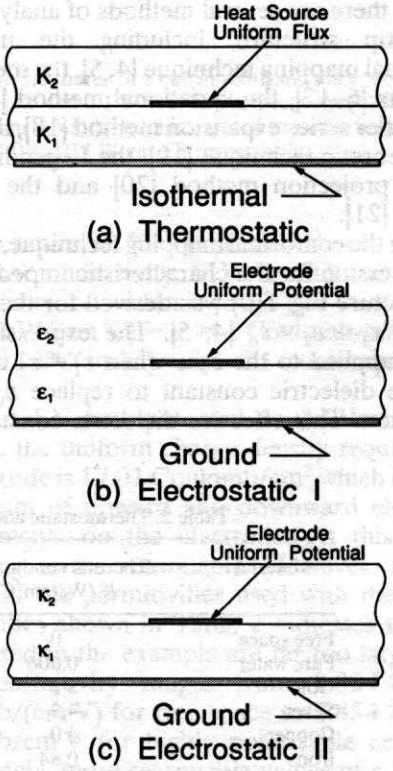

Fig. 1. Cross-section of two-dimensional thermostatic and electrostatic configurations with a strip source.

electrode, the interface between medias 1 and 2 possesses mixed boundary conditions. On the portion of interface without the electrode, the required boundary condition is the continuity of the normal

component of the electric displacement. However, the electric displacement on the electrode at the interface is unknown even though the potential on the electrode is given. This leads to difficulty in deriving an analytical solution for the potential distribution. In fact, analytical solutions for this type of problems have never been reported unless for the special cases of $\varepsilon_1 = \varepsilon_2$.

The most important application of the electrostatics I shown in Fig. 1(b) probably is the analysis of microstrip under quasi-TEM approximation [1, 2]. Usually the first layer is the substrate onto which an electrode is deposited and the second layer is the free space. The substrate is mounted on a metal housing which is also the electrical ground. Consequently, the microstrip becomes a transmission line for carrying RF or microwave signals. The microstrip structure does not support pure TEM mode, pure TE mode or pure TM mode. Rather, it supports only hybrid modes. However, in actual applications, the substrate thickness is made much smaller than the wavelengths of the RF signals to reduce dispersion and device size. As a result, the hybrid mode behaves very similarly to a TEM mode and can be seen as a quasi-TEM mode. Using quasi-TEM approximation, the structure may be satisfactorily analysed on the basis of line voltage and current. Accordingly, the problem reduces to an electrostatic one. In electrostatic approximation, there are several methods of analysing the microstrip structure, including the modified conformal mapping technique [4, 5], the method of moments [6–12], the variational method [13–17], the Fourier series expansion method [18], the function–theoretic technique [19], the Legendre polynomial projection method [20] and the unified method [21].

Using the conformal mapping technique, analytical expression for the characteristic impedance of the structure Fig. 1(b) was derived for the special case of $\varepsilon_1 = \varepsilon_2 \equiv \varepsilon_0$ [4, 5]. The expression was further applied to the case when $\varepsilon_1 \neq \varepsilon_2$ using an effective dielectric constant to replace ε_0 in the expression. This effective dielectric constant is a function of the microstrip geometry and requires numerical techniques to calculate. Thus, the modified conformal mapping technique is not a truly analytical method. Analytical solution of the microstrip structure has thus never been reported except for the special case of $\varepsilon_1 = \varepsilon_2$. On the other hand, if the prescribed condition on the strip electrode is uniform charge density rather than potential, the analytical solution for the structure has been reported [21]. Using this analytical solution with the method of moments, the structure with prescribed potential on the electrode can be solved [21].

To elaborate the analogous concept of thermostatics and electrostatics, we used the technique to be presented in the next two sections to calculate the temperature distribution of the two-layer structure depicted in Fig. 1(a) and the potential distribution of the structure in Fig. 1(b). Two types of boundary conditions on the source are studied. One type is known temperature and the other is known heat flux. For illustration purposes it is assumed that the top surface of the structure is adiabatic and the bottom surface is isothermal. For thermostatics, adiabatic boundary means zero heat flux over the boundary. In practice, adiabatic condition is achieved by having a good thermal insulator such as ambient above the boundary. The electrostatic equivalence of an adiabatic boundary is zero electric displacement over the boundary, as can be seen from Table 1. This equivalence requires the space above the top surface of the structure to have zero permitivity. In practice, permitivity can never be zero unless at some fixed frequencies. Thus, in true electrostatics, zero permitivity is not realizable. Accordingly, the electrostatic equivalence of an adiabatic boundary is hypothetical and serves only to exhibit the concept of analogy. For convenience, Table 2 lists the thermal conductivity, the electrical permitivity and the electrical conductivity of representative materials.

Figure 2(a) shows the calculated temperature distribution with a known uniform heat flux on the

Table 2. Thermostatic and electrostatic properties of representative materials

Material	Thermal conductivity K (W/(cm°C))	Electrical permitivity ε (Coulomb/(cm V))	Electrical conductivity κ (A/(cm V))
Free space	0	8.854×10^{-14} ($=\varepsilon_0$)	0
Pure water	0.006	$81\varepsilon_0$	5.5×10^{-8}
Gold	3.2	NA	4.6×10^{5}
Silver	4.3	NA	6.2×10^{5}
Copper	4.0	NA	5.9×10^{5}
Iron	0.84	NA	1.0×10^{5}
Silicon	1.5	$11.9\varepsilon_0$	4.3×10^{-6}*
GaAs	0.46	$13.1\varepsilon_0$	10^{-8}*
Glass (Pyrex)	0.011	$5.1\varepsilon_0$	$<10^{-18}$
Quartz	0.014	$3.7\varepsilon_0$	$<10^{-18}$
Sapphire	0.25	$10\varepsilon_0$	$<10^{-14}$

NA, not applicable.

* The conductivity is the intrinsic conductivity of pure semiconductors. In practice, the conductivity is increased by doping impurities and can go as high as 10^3 A/cm V.

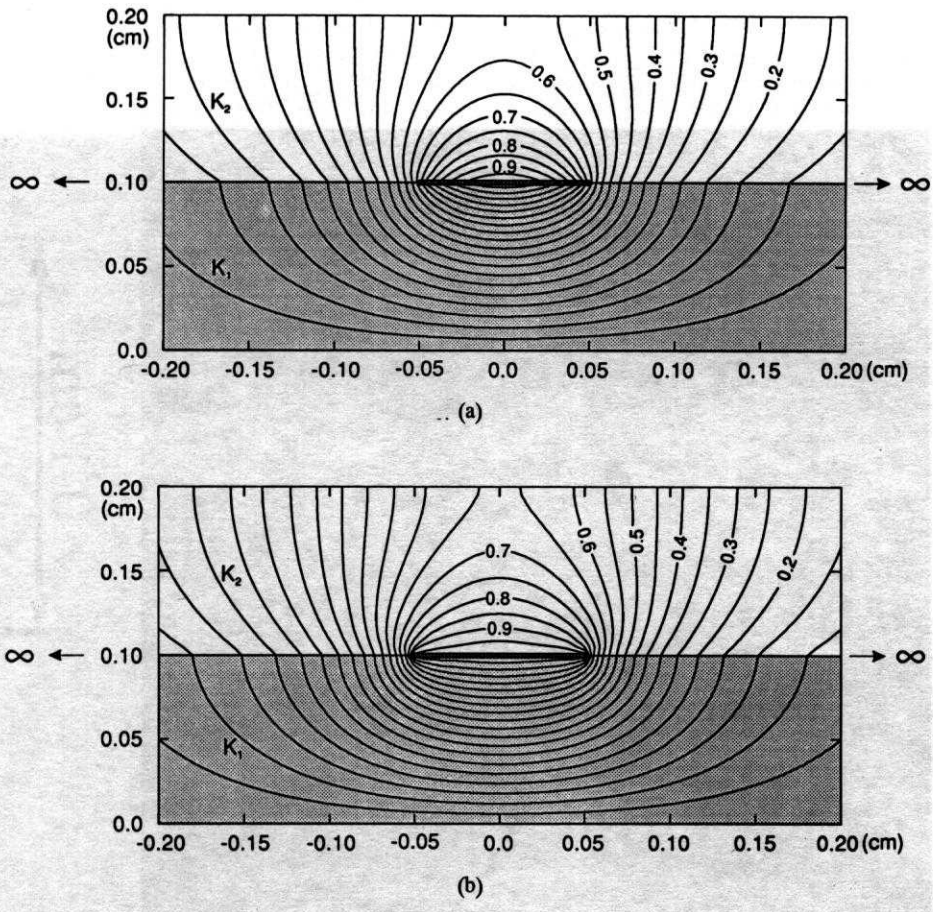

Fig. 2. (a) Calculated temperature distribution with a uniform known heat flux on the source of 1 mm in width and thickness of 1 mm for both first and second layers. The thermal conductivities of layers 1 and 2 are 1.0 and 0.1 W/(cm °C), respectively. (b) Calculated temperature distribution with a uniform temperature of 1 °C on the source of 1 mm in width and thickness of 1 mm for both first and second layers. The thermal conductivities of layers 1 and 2 are 1.0 and 0.1 W(cm °C), respectively.

source of 1 mm in width. The thicknness of the first and second layers is also 1 mm. The flux is adjusted to give a peak temperature of 1 °C on the source with respect to the isothermal bottom surface. The thermal conductivities, K_1 and K_2 are 1 and 0.1 W/(cm °C), respectively. To give the 1 °C peak temperature, the required heat flux is 17.01 W/cm^2. Figure 2(b) displays the temperature distribution of the same structure except that the source has a uniform temperature of 1 °C. Figure 3(a) and (b) gives a field presentation of Fig. 2(a) and (b), respectively. The arrows represent the negative temperature gradient and the brightness indicates the magnitude of the temperature. Once the peak temperature on the source is determined or given, the temperature distributions depend only on the ratio of K_1 to K_2 rather than on the absolute value of K_1 and K_2. Thus, if both K_1 and K_2 change by the same factor, the temperature distributions will not change. However, the required heat flux on the source to keep the temperature distributions will increase in proportion to the factor by which K_1 and K_2 increase.

To convert the temperature distributions in Fig. 2 into electrostatic equivalence, we make the following translations:

Temperature, T, °C → potential, V, volt
Thermal conductivity, K, W/(cm °C) → electrical permitivity, ε, Coulomb/(cm V)
$K_1 = 1$ W/(cm °C) → $\varepsilon_1 = 1$ Coulomb/(cm V)
$K_2 = 0.1$ W/(cm °C) → $\varepsilon_2 = 0.1$ Coulomb/(cm V)

To have a 1 V peak potential on the electrode of Fig. 2(a), the uniform charge density required on the electrode is 17.01 Coulomb/cm^2 which is equal to the sum of upward and downward electrical displacements on the electrode. At this point, everything seems reasonable. However, a comparison of the permitivities used with the actual permitivities shown in Table 2 indicates that the values used in the example are far too large. The actual permitivity ranges from 8.854×10^{-14} Coulomb/(cm V) for free space to 8.854×10^{-10} Coulomb/cm V for highly polarizable ceramics. Accordingly, more reasonable values of ε_1 and ε_2 are $\varepsilon_1 = 1 \times 10^{-12}$ Coulomb/(cm V) and $\varepsilon_2 = 0.1 \times 10^{-12}$ Coulomb/(cm V). The corresponding charge density required on the electrode of Fig. 2(a) reduces from 17.01 to 17.01×10^{-12} Coulomb/cm^2 and the peak potential on the electrode remains at 1 V.

From Fig. 2(a) we see that the potential on the

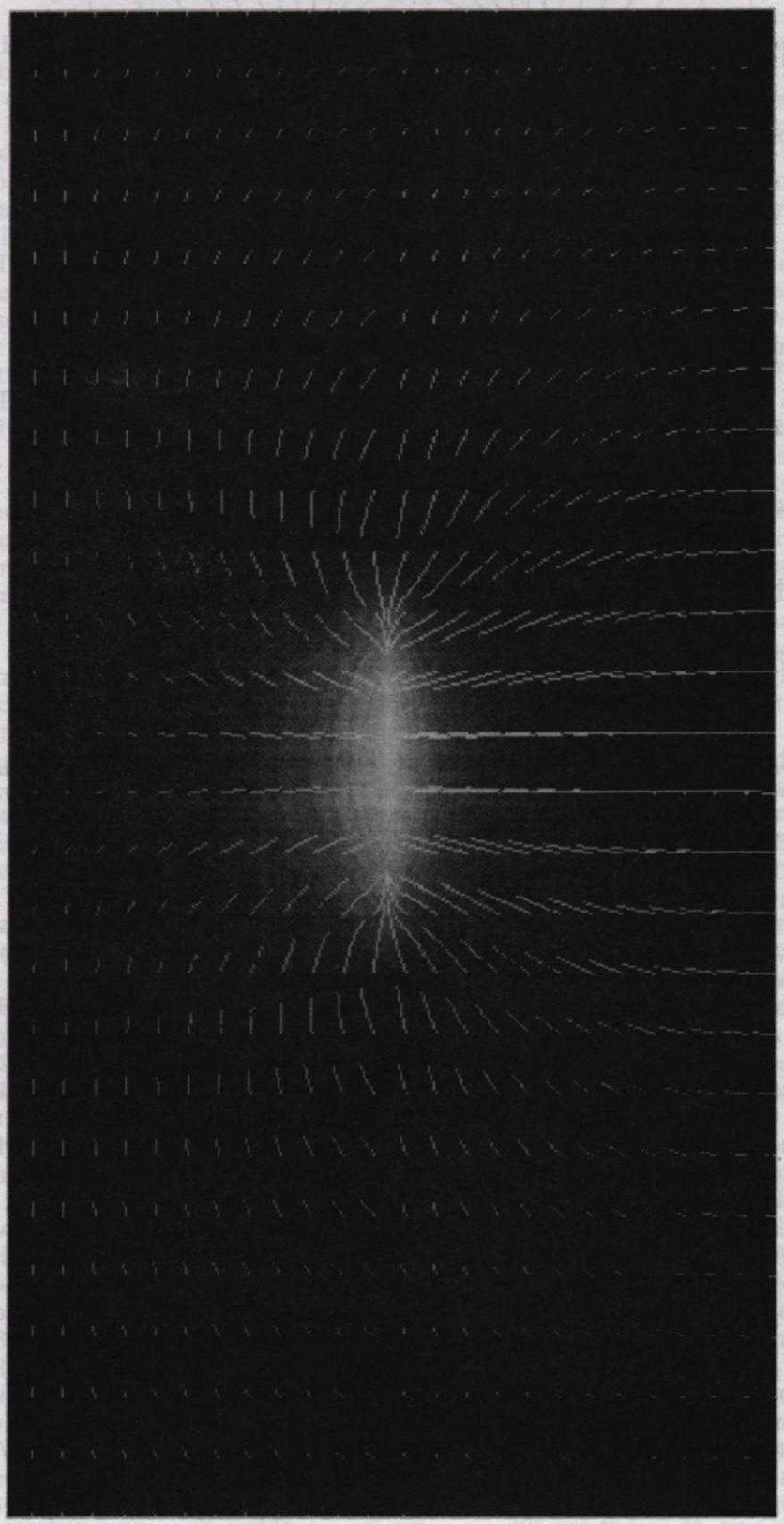

(3a)

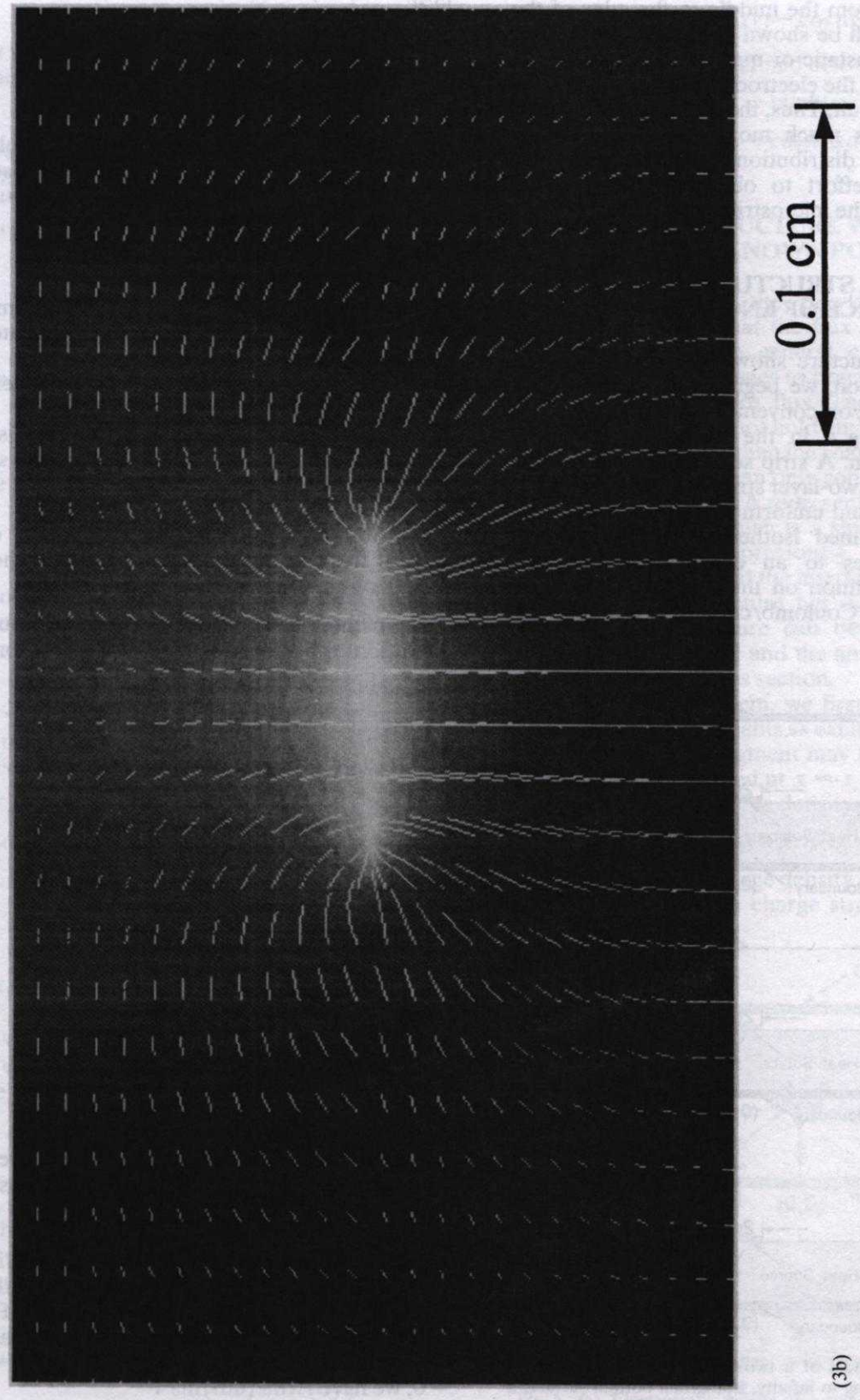

(3b)

Fig. 3. (a) Field representation of Fig. 2(a). The arrows represent the negative temperature gradient and the brightness represents the magnitude of the temperature. (b) Field representation of Fig. 2(b). The arrows represent the negative temperature gradient and the brightness represents the magnitude of the temperature.

electrode is non-uniform if the charge density is uniform. In Fig. 2(b), we observe that the uniform potential on the electrode leads to a non-uniform charge density distribution which increases nearly exponentially from the middle to the edge of the electrode, as will be shown in a later section. For practical electrostatic or quasi-static devices, it is the potential on the electrode that is controlled by the external circuit. Thus, the uniform potential on the electrode is much more common than the uniform charge distribution. In fact, it requires a great deal of effort to obtain uniform charge distribution on the microstrip electrode.

TWO-LAYER STRUCTURE WITH A STRIP SOURCE OF KNOWN FLUX

Since the structure shown in Fig. 1(a) has an analytical solution, we begin our discussion with this structure. For convenience, the structure is exhibited in Fig. 4 in the form of modeling a thermal problem. A strip source is located at the interface of the two-layer structure. The source has a width of 2ω and uniform flux of F. The bottom surface is assumed isothermal. If this thermal model translates to an electrostatic one, the equivalent condition on the source is a uniform charge density (Coulomb/cm^2). The thermal conductivity of each layer is K_1 and K_2. The lateral boundaries extend to infinity. For structure with finite lateral boundaries, the lateral boundaries can be taken into account using the method of images [22].

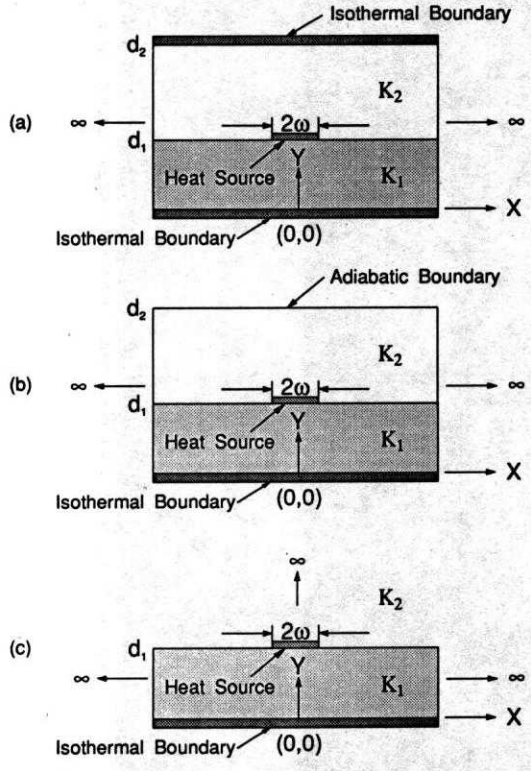

Fig. 4. Thermal model of a two-layer structure with lateral boundaries extending to infinity, isothermal bottom surface, a heat source of width 2ω and uniform flux F. The three configurations are (a) structure with isothermal top surface, (b) structure with adiabatic top surface and (c) structure with open top surface.

The governing Laplace equation is

$$\nabla^2\Psi(x,y)=\frac{\partial^2\Psi}{\partial x^2}+\frac{\partial^2\Psi}{\partial y^2}=0 \qquad (1)$$

where $\Psi(x,y)$ is the temperature. We first solve the structure for which the top surface is also isothermal as depicted in Fig. 4(a). The boundary conditions of this structure are given below.

1. The temperature approaches zero as x approaches infinity.
2. The top and bottom surfaces are isothermal.
3. The temperature is continuous at the interface between layers.
4. Tangential component of the temperature gradient is continuous at the interface.
5. Normal component of the heat flux is continuous at the interface except at the source position.
6. The heat flux on the source is uniform.
7. On the source, the normal component of the heat flux has a discontinuity equal to the heat flux of the source.

In mathematical description, these boundary conditions translate to the following equations:

$$\frac{\partial\Psi^{(i)}}{\partial x}=0 \qquad i=1,2, \text{ at } x=0 \text{ and as } x\to\infty \qquad (2)$$

$$\Psi^{(i)}=0 \qquad i=1,2 \text{ as } x\to\infty \qquad (3)$$

$$\Psi^{(1)}=0 \qquad \text{at } y=0 \qquad (4)$$

$$\Psi^{(2)}=0 \qquad \text{at } y=d_2 \qquad (5)$$

$$\Psi^{(1)}(x,y)=\Psi^{(2)}(x,y) \text{ at } y=d_1 \qquad (6)$$

$$\frac{\partial\Psi^{(1)}}{\partial x}=\frac{\partial\Psi^{(2)}}{\partial x} \qquad \text{at } y=d_1 \qquad (7)$$

$$K_1\frac{\partial\Psi^{(1)}}{\partial y}-K_2\frac{\partial\Psi^{(2)}}{\partial y}=\begin{cases}0; |x|>\omega \text{ and } y=d_1\\ F; |x|\leqslant\omega \text{ and } y=d_1\end{cases} \qquad (8)$$

where $\Psi^{(i)}$ is the temperature in the ith layer, F is the heat flux of the source, d_1 is the thickness of the first layer and (d_2-d_1) is the thickness of the second layer.

Because of the symmetry of the structure, the plane at $x=0$ is adiabatic, which suggests that we take the Fourier cosine transform of Eq. 1. Integrating by parts and using the conditions that $\Psi(x,y)\to 0$ and $\partial\Psi/\partial x\to 0$ as $x\to\infty$ and $\partial\Psi/\partial x=0$ at $x=0$, we have

$$\psi(\alpha,y)-\frac{1}{\alpha_2}\frac{d^2\psi(\alpha,y)}{dy^2}=0 \qquad (9)$$

where $\psi(\alpha, y)$ is the transform temperature expressed by

$$\psi^{(i)}(\alpha, y) = \int_0^\infty \Psi^{(i)}(x, y)\cos(\alpha x)\mathrm{d}x \quad (10)$$

and α is the spatial frequency. The solution of Eq. 9 has the form of

$$\psi^{(i)}(\alpha, y) = A\sin h(\alpha y) + B\cos h(\alpha y) \quad (11)$$

After applying the transform boundary conditions, we obtain

$$\psi^{(1)}(\alpha, y) = \frac{F\sin(\alpha\omega)\sin h(\alpha y)}{\alpha^2\cos h(\alpha d_1)\left[K_1 - K_2\dfrac{\beta}{\gamma}\right]} \quad (12)$$

and

$$\psi^{(2)}(\alpha, y) = \frac{F\sin(\alpha\omega)}{\alpha^2\cos h(\alpha d_1)(K_1\gamma - K_2\beta)} \times [\sin h(\alpha y) - \tan h(\alpha d_2)\cos h(\alpha y)] \quad (13)$$

where β and γ are defined below,

$$\beta = 1 - \tan h(\alpha d_2)\tan h(\alpha d_1) \quad (14)$$

$$\gamma = 1 - \tan h(\alpha d_2)\cot h(\alpha d_1) \quad (15)$$

The solution in the spatial domain is then obtained by the inverse Fourier cosine transform given by

$$\Psi^{(i)}(x, y) = \frac{2}{\pi}\int_0^\infty \psi^{(i)}(\alpha, y)\cos(\alpha x)\mathrm{d}\alpha \quad (16)$$

If the top surface of the structure is adiabatic rather than isothermal as shown in Fig. 4(b), the solution of Eq. 9 becomes

$$\psi^{(1)}(\alpha, y) = \frac{F\sin(\alpha\omega)\sin h(\alpha y)}{\alpha^2\cos h(\alpha d_1)\left[K_1 - K_2\dfrac{\rho}{\xi}\right]} \quad (17)$$

and

$$\psi^{(1)}(\alpha, y) = \frac{F\sin(\alpha\omega)}{\alpha^2\cos h(\alpha d_1)(K_1\xi - K_2\rho)} \times [\cos h(\alpha y) - \tan h(\alpha d_2)\sin h(\alpha y)] \quad (18)$$

where ρ and ξ are defined as

$$\rho = \tan h(\alpha d_1) - \tan h(\alpha d_2) \quad (19)$$

$$\xi = \cot h(\alpha d_1) - \tan h(\alpha d_2) \quad (20)$$

If the top surface is open as exhibited in Fig. 4(c), the thickness of the second layer approaches infinity, i.e. $d_2 \to \infty$. Applying this condition to Eqs 12 and 13 or Eqs 17 and 18, the solutions for the isothermal top surface and the adiabatic top surface configurations degenerate into the same solution given below,

$$\psi^{(1)}(\alpha, y) = \frac{F\sin(\alpha\omega)\sin h(\alpha y)}{\alpha^2\cos h(\alpha d_1)[K_1 + K_2\tan h(\alpha d_1)]} \quad (21)$$

and

$$\psi^{(2)}(\alpha, y) = \frac{F\sin(\alpha\omega)}{\alpha^2\cos h(\alpha d_1)(K_1\gamma_0 - K_2\beta_0)} \times [\sin h(\alpha y) - \cos h(\alpha y)] \quad (22)$$

where β_0 and γ_0 are defined below.

$$\beta_0 = 1 - \tan h(\alpha d_1) \quad (23)$$

$$\gamma_0 = 1 - \cot h(\alpha d_1) \quad (24)$$

TWO-LAYER STRUCTURE WITH A STRIP SOURCE OF KNOWN POTENTIAL

The solutions in the previous section are obtained assuming that the flux on the source is uniform. This is the general case for thermal problems. When it comes to practical electrostatic problems, the uniform flux (charge density for electrostatics I) does not hold any more. Instead, it is the potential rather than the charge density which is known. In fact, we can only control the potential in practical problems. A representative structure is shown in Fig. 5(a) which is a shielded microstrip line. As indicated previously, due to mixed boundary conditions at the interface, the analytical solution of this structure has not been derived. However, the structure can be solved using a discretization method and the analytical solutions derived in the previous section.

To solve the problem, we first divide the strip electrode into N segments as exhibited in Fig. 5(b). The width of each segment may be different. The ith segment is centered at $x = x_i$ and assigned an unknown uniform charge density given by

$$\sigma(\chi_i) \equiv \lambda_i \times U \quad (25)$$

where U is a unity charge density and λ_i represents the unknown relative charge strength on the ith

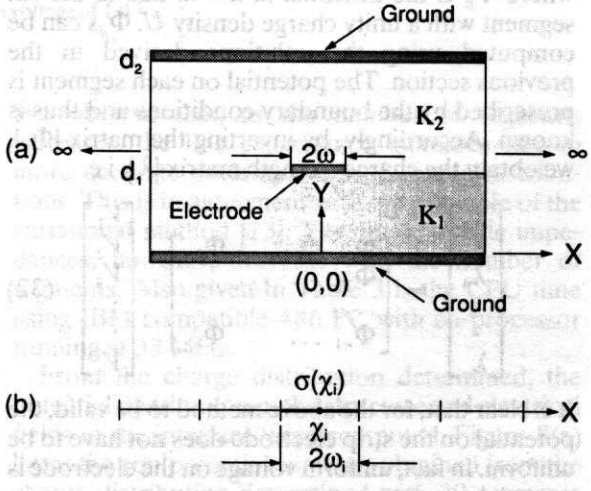

Fig. 5. (a) Electrostatic model of a two-layer structure. The lateral boundaries extend to infinity. The top and bottom surfaces are grounded. The electrode has a width of 2ω and a potential V. (b) Segmentation of the strip electrode.

segment yet to be determined. First, consider a case where only the ith segment is present and it has a unity charge density U. The potential at the interface between the first and second layers due to this ith segment can be computed using the solutions Eqs 12 and 13 derived in the previous section. Using $\Phi_i(x, d_1)$ to denote this potential, then the potential due to the ith segment having a charge density $\sigma(\chi_i) \equiv \lambda_i \times U$ can be expressed by

$$\text{Potential due to the } i\text{th segment} = \Phi_i(x, d_1)\lambda_i \tag{26}$$

Based on the superposition principle, the potential produced by all N segments is thus given by

$$V(x) = \sum_{i=1}^{N} \Phi_i(x, d_1)\lambda_i \tag{27}$$

Apparently, the potential $V(x)$ over the electrode must satisfy the prescribed potential. In Eq. 27, since we have N unknown λ_is, we need to specify $V(x)$ over the electrode only at N locations. For simplicity, we specify $V(x)$ at the middle of each segment and define it as

$$V_j \equiv V(x)|_{x=x_j} \tag{28}$$

Substituting Eq. 28 into Eq. 27 yields

$$V_j = \sum_{i=1}^{N} \Phi_i(x_j, d_1)\lambda_i \equiv \sum_{i=1}^{N} \Phi_{ji}\lambda_i \tag{29}$$

where

$$\Phi_{ji} \equiv \Phi_i(x_j, d_1) \tag{30}$$

Rewriting Eq. 30 in matrix form yields

$$\begin{bmatrix} V_1 \\ V_2 \\ V_3 \\ \cdot \\ \cdot \\ V_n \end{bmatrix} = \begin{bmatrix} \Phi_{11} & \Phi_{12} & \cdots & \Phi_{1n} \\ \Phi_{21} & \cdots & \cdots & \\ \cdots & & & \\ \Phi_{n1} & \cdots & & \Phi_{nn} \end{bmatrix} \begin{bmatrix} \lambda_1 \\ \lambda_2 \\ \lambda_3 \\ \cdot \\ \cdot \\ \lambda_n \end{bmatrix} \tag{31}$$

where Φ_{ji} is the potential at $x = x_j$ due to the ith segment with a unity charge density U. Φ_{ji}s can be computed using the solutions derived in the previous section. The potential on each segment is prescribed by the boundary conditions and thus is known. Accordingly, by inverting the matrix $[\Phi_{ji}]$, we obtain the charge strength matrix $[\lambda_i]$, i.e.

$$\begin{bmatrix} \lambda_1 \\ \lambda_2 \\ \lambda_3 \\ \cdot \\ \cdot \\ \lambda_n \end{bmatrix} = \begin{bmatrix} \Phi_{11} & \Phi_{12} & \cdots & \Phi_{1n} \\ \Phi_{21} & \cdots & \cdots & \\ \cdots & & & \\ \Phi_{n1} & \cdots & & \Phi_{nn} \end{bmatrix}^{-1} \begin{bmatrix} V_1 \\ V_2 \\ V_3 \\ \cdot \\ \cdot \\ V_n \end{bmatrix} \tag{32}$$

It is clear that, for the above method to be valid, the potential on the strip electrode does not have to be uniform. In fact, uniform voltage on the electrode is a special case.

After the charge density of each segment is obtained, the potential at any given point within the structure is expressed by

$$\Psi(x, y) = \sum_{i=1}^{N} \lambda_i \Phi_i(x, y) \tag{33}$$

And the electric field is given by

$$E(x, y) = -\nabla\Psi(x, y) \tag{34}$$

The characteristic impedance of the microstrip is then calculated using the expression

$$Z_0 = \frac{1}{v_0\sqrt{CC_0}} \text{ (ohms)} \tag{35}$$

where v_0 is the speed of light in free space, C_0 is the capacitance per unit length of the microstrip with all layers replaced by free space and C is the capacitance per unit length of microstrip with dielectric structure. The capacitance per unit length is the total charge per unit length divided by the potential of the strip conductor, namely,

$$C = \frac{\sum_{i=1}^{N} \sigma(\chi_i) 2\omega_i}{V} \text{ (Farads/cm)} \tag{36}$$

where $2\omega_i$ is the width of the ith segment.

AN ELECTROSTATIC EXAMPLE

To illustrate the method presented, we solve an electrostatic two-layer structure shown in Fig. 5(a). The first layer is 250 μm thick alumina substrate and the second layer is 2 mm thick free space. A 250 μm wide electrode is located on the substrate. The relative permitivities of the free space and the alumina are 1.0 and 10.0 respectively. The top and bottom surfaces are electrically grounded and the lateral boundaries extend to infinity. This structure represents a typical microstrip transmission line.

For the problem on hand, it is the voltage rather than the charge density on the electrode that is given. We first need to divide the electrode into elements. Segmentation of the electrode needs not be equally spaced. Several schemes of discretizing the electrode were studied to identify an optimal one. Figure 6(a) exhibits the resulting charge distributions on the electrode which is equally divided into 16 segments and 100 segments, respectively. The voltage on the electrode is 1.0 V. We see that the charge distribution is very non-uniform near the edges of the electrode. Apparently, equal discretization is not an efficient scheme. Figure 6(b) displays the charge distribution on the same electrode which is divided exponentially into only eight segments. To compare the accuracy of the equal and exponential discretizations, the potentials on the electrode and the dielectric interface were computed using the corresponding charge distributions obtained. The results are shown in Fig. 7 where the potential attained with equal discretization of 100 segments is plotted as a reference. We see that discretization of 100 segments results in a potential on the

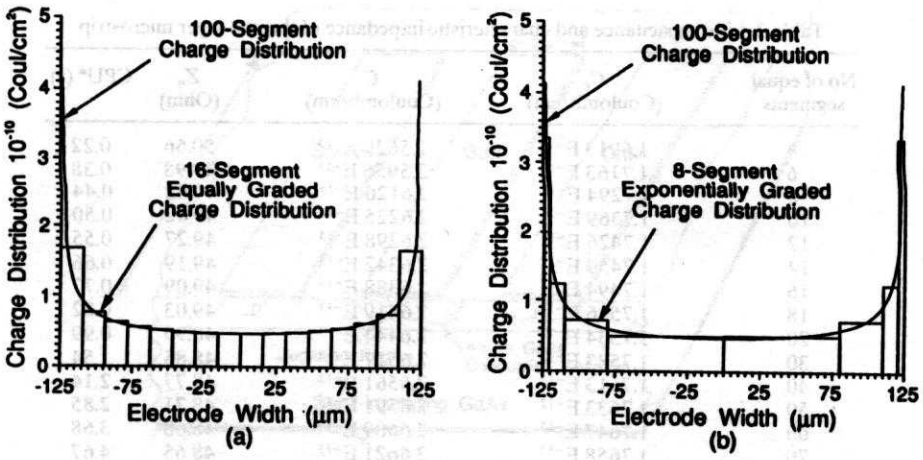

Fig. 6. Computed charge distributions on the strip electrode at 1.0 V of constant voltage for the two-layer structure example. (a) Equal discretization into 16 segments and 100 segments. (b) Exponential discretization into eight segments.

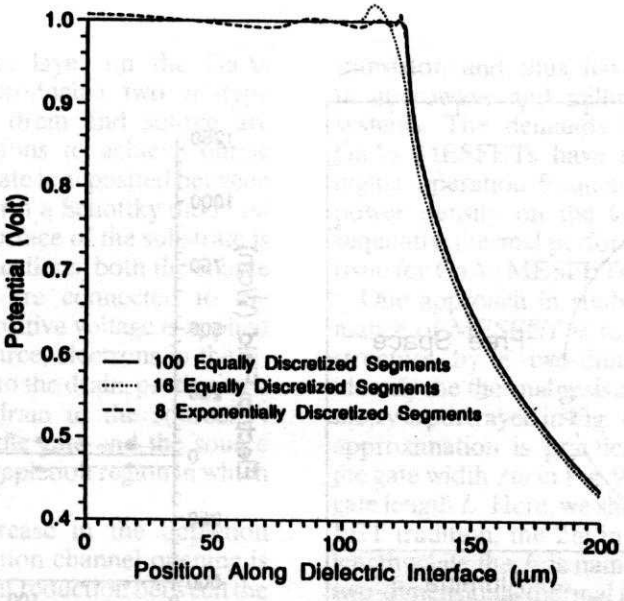

Fig. 7. Potential on the electrode and dielectric interface obtained using the charge distributions computed with the equal discretization of 16 segments, exponential discretization of eight segments and equal discretization of 100 segments. The boundary condition on the electrode is a constant voltage of 1.0 V.

electrode which perfectly satisfies the boundary condition of 1.0 V on the electrode. It is also seen that the exponential discretization of eight segments gives a more accurate result than that obtained from equal discretization of 16 segments. Other schemes have also been tried. It was concluded that exponential discretization appears to be the most effective one for microstrips.

Once the charge distributions were calculated, the line capacitances were obtained using Eq. 36. The results are presented in Table 3 for a different number of segments in the equal discretization scheme. Notice that C_0 is the line capacitance with the alumina substrate replaced by free space and C is the line capacitance of the structure with alumina substrate. The characteristic impedances were also calculated using Eq. 35 and are shown in Table 3. We observe that, as the number of segments increases, the line capacitance increases due to more accurate determination of charge distributions. This is in agreement with the principle of the variational method [13]. The characteristic impedances, however, decrease with the number of segments. Also given in Table 3 is the CPU time using IBM compatible 486 PC with co-processor running at 33 MHz.

From the charge distribution determined, the potential distribution in the structure and electrical fields at the interface were computed. Figure 8(a) limns the equipotential contours obtained from the charge distribution determined with 20 segments of exponential discretization. Figure 8(b) shows the electric fields at the interface between the alumina substrate and the free space. E_x is the tangential

Table 3. Line capacitance and characteristic impedance of the two-layer microstrip

No of equal segments	C_0 (Coulomb/cm)	C (Coulomb/cm)	Z_0 (Ohm)	CPU* (s)
4	1.6913 E^{-12}	2.5629 E^{-13}	50.66	0.22
6	1.7163 E^{-12}	2.5956 E^{-13}	49.98	0.38
8	1.7294 E^{-12}	2.6126 E^{-13}	49.62	0.44
10	1.7369 E^{-12}	2.6225 E^{-13}	49.42	0.50
12	1.7426 E^{-12}	2.6298 E^{-13}	49.27	0.55
14	1.7459 E^{-12}	2.6342 E^{-13}	49.19	0.66
16	1.7494 E^{-12}	2.6388 E^{-13}	49.09	0.77
18	1.7516 E^{-12}	2.6419 E^{-13}	49.03	0.82
20	1.7534 E^{-12}	2.6444 E^{-13}	48.99	0.99
30	1.7583 E^{-12}	2.6517 E^{-13}	48.85	1.54
40	1.7613 E^{-12}	2.6561 E^{-13}	48.77	2.14
50	1.7633 E^{-12}	2.6591 E^{-13}	48.71	2.85
60	1.7647 E^{-12}	2.6609 E^{-13}	48.68	3.68
70	1.7658 E^{-12}	2.6621 E^{-13}	48.65	4.67
80	1.7668 E^{-12}	2.6629 E^{-13}	48.63	5.83
100	1.7683 E^{-12}	2.6635 E^{-13}	48.60	8.73

* CPU time measured using IBM compatible 486 PC with co-processor running at 33 MHz.

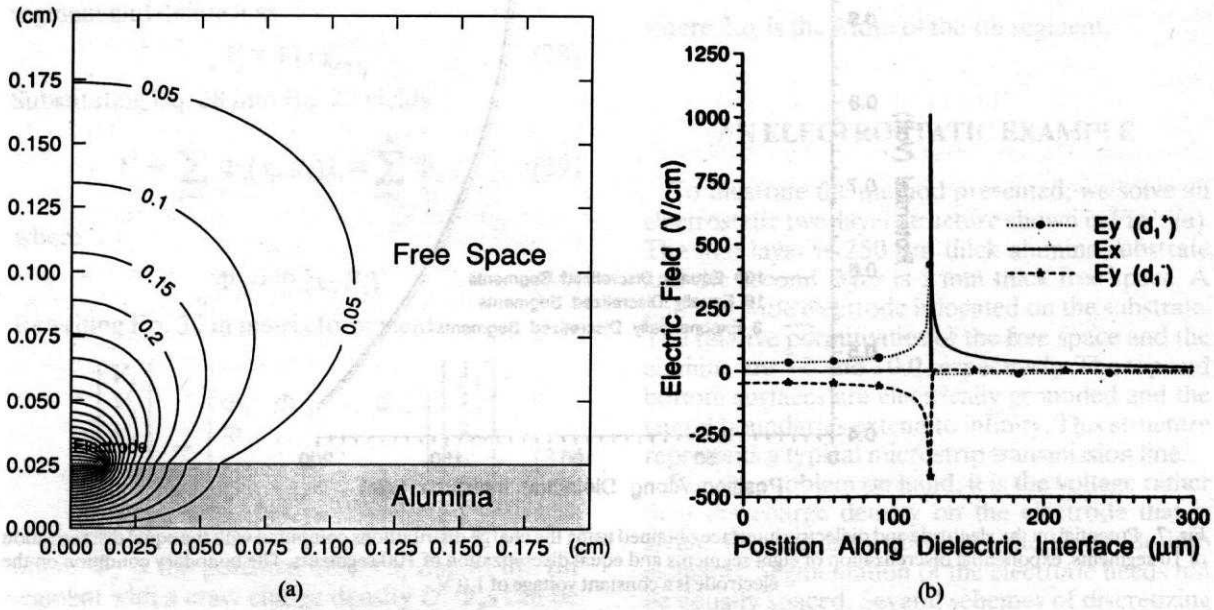

Fig. 8. (a) Equipotential contours in the cross-section of the two-layer structure example. The unit of contours is in volts. (b) Magnitude of the electric fields on the electrode and along the dielectric interface. E_x is the tangential component. $E_y(d_1^+)$ is the normal component right above the interface and $E_y(d_1^-)$ is that right below the interface.

component of the electric field, $E_y(d_1^+)$ is the normal component right above the interface and $E_y(d_1^-)$ is that right below the interface. We see that E_x is zero on the electrode, as anticipated. Near the electrode edge, however, E_x increases drastically and reaches a peak value right at the edge. This peak value is ~1000 V/cm for an electrode voltage of 1.0 V. It increases in proportion to the electrode voltage and may cause corono discharge or dielectric breakdown for high applied voltage. Right above the electrode, the normal component is positive and thus the field aims upward. Right below the electrode, it is negative and the field points downward. At some distance away from the electrode, both $E_y(d_1^+)$ and $E_y(d_1^-)$ become negative and the electric flux lines begin heading downward at the interface. From the magnitude of $E_y(d_1^+)$ and $E_y(d_1^-)$, one may also calculate the total charge density along the interface, which includes both the free charge and the bound charge.

A THERMOSTATIC EXAMPLE

The thermostatic example is a metal–semiconductor field effect transistor (MESFET) built on semi-insulating gallium arsenide (GaAs) substrate as depicted in Fig. 9. The device is fabricated by

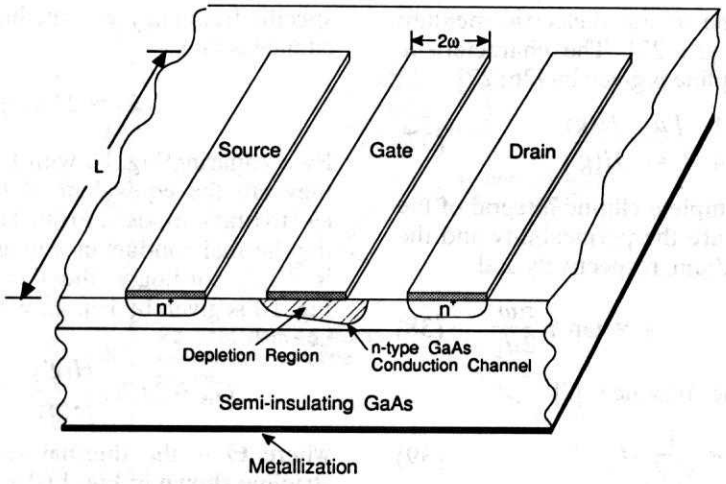

Fig. 9. Physical structure of a GaAs field effect transistor using Schottky diode as a gate. Here 2ω is the gate width and L the gate length.

growing an n-type GaAs layer on the GaAs substrate, followed by producing two n^+-type regions. Metal pads for drain and source are deposited on the n^+ regions to achieve ohmic contact. A metal strip for gate is deposited between the drain and source to form a Schottky diode on the n-layer. The bottom surface of the substrate is metallized. In typical applications, both the source and the bottom surface are connected to the electric ground. When a positive voltage is applied between the drain and source, electrons in the n-layer flow from the source to the drain, producing a current going from the drain to the source. A positive voltage between the gate and the source increases the depth of the depletion region in which electrons are depleted.

Due to the depth increase in the depletion region, the n-type conduction channel opening is reduced, resulting in current reduction between the drain and the source. Thus, the gate voltage controls the drain to source current. Due to the high mobility of electrons in GaAs, MESFETs built on GaAs have a higher speed than silicon transistors and, thus, have important applications in microwave and millimeter-wave devices and systems. The demands on the performance of GaAs MESFETs have been higher power and higher operation frequency. This leads to higher power density on the GaAs device chip. Consequently, thermal performance becomes a critical issue for GaAs MESFETs [23, 24].

One approach in studying the thermal performance of MESFET is to approximate the device structure by a two-dimensional geometry and identify the thermal resistance. The simplified geometry is portrayed in Fig. 10. This two-dimensional approximation is practically reasonable because the gate width 2ω in Fig. 9 is much smaller than the gate length L. Here, we should point out that, in the FET tradition, the 2ω in Fig. 9 is called the gate length while the L is named the gate width. In the two-dimensional thermal model of Fig. 10, the gate is treated as a strip surface heat source because most of the heat is generated right underneath the gate electrode. One method of finding the thermal resistance is to utilize the model for the shielded

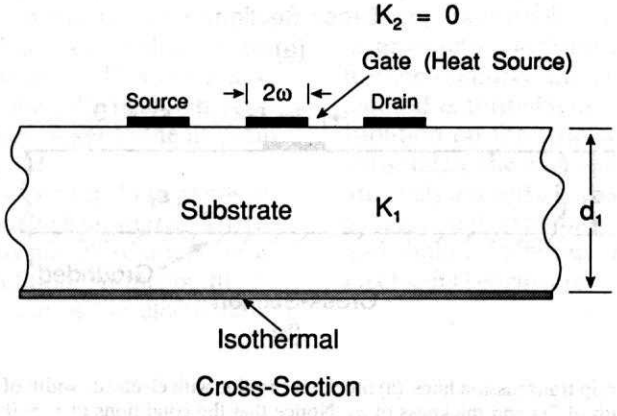

Fig. 10. Two-dimensional FET thermal model.

strip transmission line in the dielectric medium shown in Fig. 11(a) [25–27]. The characteristic impedance of the stripline is given by [26, 27]

$$Z_1 = \frac{1}{4}\sqrt{\frac{\mu_1}{\varepsilon_1}}\,\frac{H(g)}{H(g')} \tag{37}$$

where $H(g)$ is the complete elliptic integral of the first kind, μ_1 and ε_1 are the permeability and the permitivity of the medium, respectively and

$$g = \sec h\,\frac{\pi\omega}{2d_1} \qquad g' = \tan h\,\frac{\pi\omega}{2d_1} \tag{38}$$

The capacitance of the stripline is [2]

$$C_1 = \frac{1}{V_p Z_1} L \tag{39}$$

where L is the length of the stripline and

$$V_p = \frac{1}{\sqrt{\mu_1\varepsilon_1}} \tag{40}$$

is the phase velocity of the electromagnetic wave propagating along the stripline. Substituting Eqs 37 and 40 into Eq. 39, we obtain

$$C_1 = 4L\varepsilon_1\,\frac{H(g')}{H(g)} \tag{41}$$

In the shielded stripline shown in Fig. 11(a) the electrical field distribution is symmetrical with respect to the plane along the electrode. One-half of the stripline can be represented by the structure depicted in Fig. 11(b). In Fig. 11(b), the condition of $\varepsilon_2 = 0$ is hypothetical because $\varepsilon_2 = 0$ is not realizable unless for some specific media at a specific frequency. For the half stripline, the capacitance is thus

$$C_2 = 2L\varepsilon_1\,\frac{H(g')}{H(g)} \tag{42}$$

By comparing Fig. 10 with Fig. 11(b), we see that they are the equivalent of the thermostatic and electrostatic models. From Table 1, the analogy of the thermal conductance in an electrostatic model is C. Accordingly, the thermal conductance of Fig. 10 is given by Eq. 42 with ε_1 replaced by K_1, i.e.

$$G_{th} = 2LK_1\,\frac{H(g')}{H(g)} \quad \text{and} \quad \Theta = \frac{1}{G_{th}} \tag{43}$$

where Θ is the thermal resistance. In the half stripline shown in Fig. 11(b), the boundary condition on the electrode is uniform voltage which translates into uniform temperature for the thermal model of Fig. 10. Thus, Eq. 43 is valid for the boundary condition of uniform temperature on the heat source.

For thermostatic problems, usually it is the flux which is prescribed on the source. Thus, if uniform heat flux is given in the model of Fig. 10, its thermal resistance can be obtained using the two-layer structure shown in Fig. 4(c) by letting $K_2 = 0$. From Eq. 21, we can find $\psi^{(1)}(\alpha, y)$ for $y = d_1$ and $K_2 = 0$. Substituting $\psi^{(1)}(\alpha, d_1)$ into Eq. 16, we find the peak temperature $\Psi^{(1)}(0, d_1)$. Dividing $\Psi^{(1)}(0, d_1)$ with the source power, we obtain the thermal resistance

$$\Theta = \frac{1}{\pi LK_1}\,\frac{1}{\omega}\int_0^\infty \frac{\sin(\alpha\omega)\tan h(\alpha d_1)}{\alpha^2}\,d\alpha \tag{44}$$

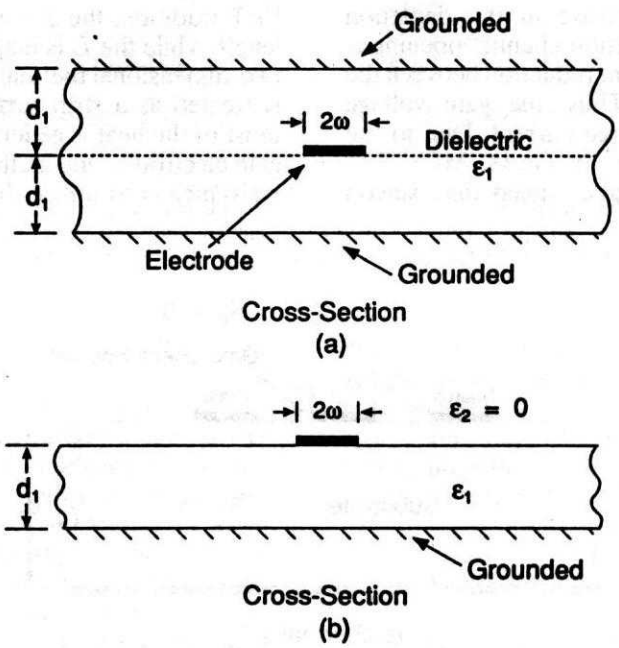

Fig. 11. Electrostatic models of strip transmission lines. (a) Shielded stripline with electrode width of 2ω and thickness of $2d_1$. (b) An open stripline with electrode width of 2ω and thickness of d_1. Notice that the conditions of $\varepsilon_2 = 0$ is hypothetical because it is not realizable in electrostatics.

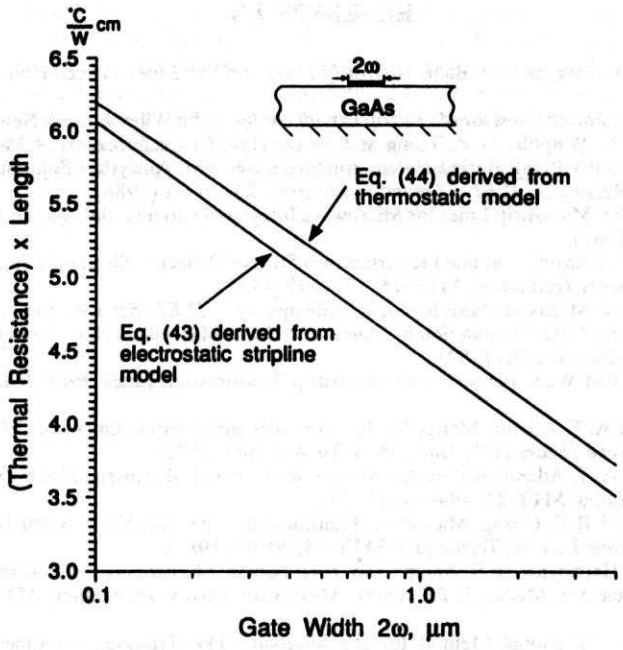

Fig. 12. Calculated results of thermal resistance–length product using Eq. 43 derived from electrostatic stripline model and Eq. 44 obtained from thermostatic model for the GaAs FET model shown.

Now we are ready to compare the thermal resistance results of Eqs 43 and 44. The example is a model of GaAs FET with a substrate thickness of 125 μm shown in Fig. 12. The results of resistance–length product are plotted in Fig. 12. We see that the thermal resistance obtained from the thermostatic model of Eq. 44 is higher. This is explained as follows. In the thermostatic models, uniform flux is prescribed and the resulting temperature on the heat source is non-uniform. The thermal resistance of Eq. 44 is derived using the peak temperature on the heat source. On the other hand, in the electrostatic stripline model which results in Eq. 43, uniform electrostatic potential is prescribed which is analogous to uniform temperature on the heat source. The thermal resistance is obtained with the uniform temperature and, thus, is lower than that of Eq. 44 which uses the peak temperature of the non-uniform temperature distribution on the source of the thermostatic case. From the results given in Fig. 12, we see that Eqs 33 and 44 are closer as the gate width 2ω becomes smaller. This is because when the gate width is smaller, the peak temperature used in Eq. 44 becomes closer to the uniform temperature utilized in Eq. 43.

The choice of using Eq. 43 or Eq. 44 depends on the prescribed condition on the heat source. Therefore, the engineers need to pay close attention to the actual heat source condition. At this point, we should point out that the use of the electrostatic stripline model gives only the thermal resistance. However, the thermostatic model not only provides a thermal resistance closer to the real situation but also enables us to calculate the temperature and flux at any locations in the structure. The temperature and flux distribution in the structure offer the engineers an opportunity as well as insight as to how the heat is transported from the source to the external boundary.

SUMMARY

In summary, we establish and present the basic analogy between thermostatics and electrostatics to enhance the understanding of both thermal and electrical problems without having to learn either thermostatics or electrostatics from scratch. To elaborate the analogy, an explicit example is given. To strengthen the link, we derive and report the analytical temperature solution of a two-dimensional two-layer structure with a strip source of known flux. To further reinforce the connection, a discretization method is formulated to calculate the charge distribution on the strip source of given voltage. To consolidate the concept, two application examples are analysed and discussed. We are certain that the analogy and examples would enhance the communication between electrical engineers and mechanical engineers.

REFERENCES

1. K. C. Gupta, R. Garg, and I. J. Bahl, *Microstrip Lines and Slot Lines*, Artech House Inc., Dedham, MA (1979).
2. T. C. Edwards, *Foundations for Microstrip Circuit Design*, John Wiley & Sons, New York (1981).
3. Z. L. Liau, J. N. Walpole, D. Z. Tsang and V. Diadiuk, Characterization of Mass-Transported P-Substrate GaInAsP/InP Buried-Heterostructure Laser with Analytical Solutions for Electrical and Thermal Resistance, *IEEE J. Quantum Electron.*, **24**, 36–42 (1988).
4. M. V. Schneider, Microstrip Lines for Microwave Integrated Circuits, *Bel. Sys. Tech. J.*, May–June, 1142–1144 (1969).
5. H. A. Wheeler, Transmission-line Properties on a Strip of Dielectric Sheet on a Plane, *IEEE Trans. Microwave Theory Techniques*, **MTT-25**, 631–647 (1977).
6. R. F. Harrington, Matrix Methods for Field Problems, *Proc. IEEE*, **55**, 136–149 (1967).
7. R. F. Harrington, *Field Computation by Moment Methods*, MacMillan, New York (1968); reprinted by Krieger, Melbourne, FL (1982).
8. P. Silvester, TEM Wave Properties of Microstrip Transmission Lines, *Proc. IEEE*, **115**, 43–47 (1968).
9. A. Farrar and A. T. Adams, Matrix Method for Microstrip Three-dimensional Problems, *IEEE Trans. Microwave Theory Techniques*, **MTT-20**, 497–504 (1972).
10. A. Farrar and A. T. Adams, A Potential Method for Covered Microstrip, *IEEE Trans. Microwave Theory Techniques*, **MTT-21**, 494–496 (1973).
11. C. E. Smith and R. S. Chang, Microstrip Transmission Line with Finite-width Dielectric, *IEEE Trans. Microwave Theories Techniques*, **MTT-28**, 90–94 (1980).
12. C. Wei, R. F. Harrington, J. R. Mautz, and T. K. Sarkar, Multiconductor Transmission Lines in Multilayer Dielectric Media, *IEEE Trans. Microwave Theory Techniques*, **MTT-32**, 439–449 (1984).
13. E. Yamashita, Variational Method for the Microstrip-like Transmission Lines, *IEEE Trans. Microwave Theory Techniques*, **MTT-16**, 529–535 (1968).
14. E. Yamashita and K. Atsuki, Strip Line with Rectangular Outer Conductor and Three Dielectric Layers, *IEEE Trans. Microwave Theory Techniques*, **MTT-18**, 238–244 (1970).
15. B. M. McDonald, M. Friedman and A. Wexler, Variational Solution of Integral Equations, *IEEE Trans. Microwave Theory Techniques*, **MTT-22**, 237–247 (1974).
16. B. Bhat and S. K. Koul, Unified Approach to Solve a Class of Strip and Microstrip-like Transmission Lines, *IEEE Trans. Microwave Theory Techniques*, **MTT-30**, 679–686 (1982).
17. E. Yamashita, H. Oshashi and K. Atsuki, Characterization of Microstrip Lines Near a Substrate Edge and Design Formulas of Edge-compensated Microstrip Lines, *IEEE Trans. Microwave Theory Techniques*, **MTT-30**, 890–896 (1989).
18. S. V. Judd, I. Whiteley, R. J. Clowes and D. C. Pickard, An Analytical Method for Calculating Microstrip Transmission Line Parameters, *IEEE Trans. Microwave Theory Techniques*, **MTT-18**, 78–87 (1970).
19. R. Mittra and T. Itoh, Charge and Potential Distribution in Shielded Striplines, *IEEE Trans. Microwave Theory Techniques*, **MTT-18**, 149–156 (1970).
20. P. Silvester and P. Benedek, Electrostatics of Microstrip—Revisited, *IEEE Trans. Microwave Theory Techniques*, **MTT-20**, 756–758 (1982).
21. C. C. Lee and Y. J. Min, A New Technique for the Electrostatic Analysis of Microstrip in Anisotropic Multi-layer Structures, *ElectroSoft J.: Adv. Electrical Engng Software*, **1**, 127–140 (1990).
22. A. L. Palisoc and C. C. Lee, Exact Thermal Representation of Multi-layer Rectangular Structures by Infinite Plate Structures Using the Method of Images, *J. Appl. Phys.*, **64**, 6851 (1988).
23. H. Fukui, Thermal Resistance of GaAs Field-effect Transistors, *IEEE Int. Electron. Devices Meet. Tech. Digest*, 118–121 (1980).
24. P. Saunier and H. Q. Tserng, AlGaAs/InGaAs Heterostructures with Doped Channels for Discrete Devices and Monolithic Amplifiers, *IEEE Trans. Electron. Devices*, **36**, 2231–2235 (1989).
25. H. F. Cook, Microwave Field Effect Transistors in 1978, *Microwave J.*, April, 43–48 (1978).
26. S. B. Cohn, Characteristic Impedance of the Shielded-transmission Line, *IRE Trans. Microwave Theory Techniques*, July, 52–57 (1954).
27. S. B. Cohn, Shielded Coupled-strip Transmission Line, *IRE Trans. Microwave Theory Techniques*, October, 29–38 (1955).

Chin C. Lee was born in Taiwan in 1948. He received his BE and MS degrees in electronics from the National Chiao-Tung University, Hsinchu, Taiwan, in 1970 and 1973, respectively and his PhD degree in electrical engineering from Carnegie-Mellon University, Pittsburgh, Pennsylvania in 1979. From 1979 to 1980, he was a research associate with the Electrical Engineering Department of Carnegie-Mellon University. From 1980 to 1983, he was with the Electrical Engineering Department of the University of California, Irvine, as a research specialist. In 1984, he joined the same department as an assistant professor and became professor of electrical and computer engineering in July 1994. He served as the graduate advisor of electrical and computer engineering at UCI from 1990/91 to 1993/94. His research interests include electronic packaging technology, thermal analysis and design of electronic devices, integrated optics, optoelectronics, electromagnetic theory, acoustic microscopy and acoustics. He has co-authored three book chapters and 85 papers in the subject areas mentioned above. Chin C. Lee is a senior member of IEEE and a member of the International Society for Boundary Elements and Tau Beta Pi. He is an Associate Editor of *IEEE Transactions on Components, Packaging and Manufacturing Technology.*

David H. Chien was born in Taiwan in 1967. He received his BS in electrical engineering (*magna cum laude*) from California State University, Los Angeles, California in 1991. He continued graduate study at University of California, Irvine and earned his MS in electrical engineering in 1992. Currently, he is working toward his PhD degree in the area of solid state devices at the University of California, Irvine. His research interests include electronic packaging technology and thermal analysis of electronic devices. He is a member of Tau Beta Pi, Eta Kappa Nu, Phi Kappa Phi and a student member of the IEEE.